Benthic fluxes of oxygen and heat from a seasonally hypoxic region of Saanich Inlet fjord observed by eddy covariance

Clare E. Reimers, Rhea D. Sanders, Richard Dewey, & Rick Noel

June 2020

Estuarine, Coastal and Shelf Science 243 (2020) 106815

Contents lists available at ScienceDirect

Estuarine, Coastal and Shelf Science

journal homepage: http://www.elsevier.com/locate/ecss

Benthic fluxes of oxygen and heat from a seasonally hypoxic region of Saanich Inlet fjord observed by eddy covariance

Clare E. Reimers [a,*], Rhea D. Sanders [a], Richard Dewey [b], Rick Noel [c]

[a] College of Earth, Ocean, and Atmospheric Sciences, Oregon State University, Corvallis, OR, 97331, USA
[b] School of Earth and Ocean Sciences, University of Victoria, PO Box 1700, Station CSC, Victoria, BC, V8W2Y2, Canada
[c] Rockland Scientific, 520 Dupplin Road, Victoria, BC, V8Z 1C1, Canada

ARTICLE INFO

Keywords:
Benthic fluxes
Eddy covariance
Observatory
Hypoxia
Turbulence
Saanich inlet

ABSTRACT

Benthic habitats within fjords are predominantly insulated from the high energy physical dynamics of open coastlines. As a result, fjords may have atypical mass and heat transfer rates at the seafloor. This study presents aquatic eddy covariance (EC) measurements made continuously from late May 2013 through December 2013, in Saanich Inlet fjord, British Columbia, to assess areal-averaged benthic fluxes of dissolved oxygen and heat, and their relationships to bottom boundary layer dynamics and water properties. The measurements were achieved by the connection of a system of underwater EC sensors to Ocean Network Canada's Victoria Experimental Network Under the Sea (VENUS) observatory that has a primary seafloor node located near the 100-m isobath in Patricia Bay off the eastern shore of Saanich Inlet. Current velocities and turbulence (characterized by turbulent kinetic energy and dissipation rate estimates) were observed to be generally low with the weakest dynamics in autumn during periods of heightened hypoxia. EC fluxes that represented turbulent eddy transport in balance with the seafloor source/sink were derived through conditional criteria that excluded measurements occurring when the bottom boundary layer was not sufficiently turbulent or when transient shifts in bottom water properties were observed. The accepted fluxes of oxygen (-1.6 ± 1.2 mmol m^{-2} d^{-1}) and heat (0.27 ± 0.57 W m^{-2}) showed only modest variations within the observed 7-month period in Saanich Inlet. Broader implications of these fluxes are that: 1) seafloor oxygen uptake rates are too limited to drive annual expansions and intensification of the site's overlying seasonal hypoxic zone, and 2) heat transferred to the seabed in summer is only slowly dissipated back to the water column during other times of the year.

1. Introduction

In shallow-water to shelf-depth aquatic systems there can be substantial variability in fluxes of solutes and heat across the sediment-water interface as benthic communities respond to changes in organic carbon inputs, flow dynamics, light, and water mass characteristics such as oxygen concentration and temperature on diurnal and seasonal time scales. The benthos of semi-enclosed coastal basins such as fjords, bays and lagoons are particularly prone to changes in terrestrial sediment delivery, water column ventilation, and biological productivity (Syvitski et al., 1987; Levin et al., 2009). These factors often shift seasonally and in response to large-to-local scale, ocean conditions (Iriarte, 2018). As a result, coastal basins are frequently sites that exhibit water column hypoxia/anoxia; where hypoxia is typically characterized by dissolved oxygen concentrations <62.5 μmol L^{-1} (1.4 mL L^{-1}), severe hypoxia occurs at <22.3 μmol L^{-1} (0.5 mL L^{-1}), and anoxia when oxygen is fully depleted (Levin et al., 2009). Coastal basins are also sensitive to climatic events such as strong El Niños (Jackson et al., 2018), and their sediments preserve indicators of environmental changes in high-resolution records (Tunnicliffe, 2000; Langton et al., 2008; Bertrand et al., 2012). Such sediments are of further interest for having the highest area-normalized annual rates of organic carbon burial globally (Smith et al., 2015).

In this study we focus on a seasonally hypoxic region of Saanich Inlet, a well-studied temperate fjord (Sato et al., 2014), to consider how deep-water renewal events, the intensity of turbulence, and properties of the soft-bottom seabed dictate benthic oxygen consumption and heat exchange at the margins of a coastal basin. Our assessments are derived from an extended time-series of in situ eddy covariance (EC) measurements made with synchronized velocity, oxygen and temperature sensors on the Victoria Experimental Network Under the Sea (VENUS)

* Corresponding author.
E-mail address: clare.reimers@oregonstate.edu (C.E. Reimers).

https://doi.org/10.1016/j.ecss.2020.106815
Received 5 February 2020; Received in revised form 24 March 2020; Accepted 30 April 2020
Available online 25 June 2020

seafloor cabled observatory array that operates within the Saanich Inlet, as part of Ocean Networks Canada (ONC). Previous monitoring and experiments within the environment surrounding the VENUS observatory have traced the effects of low dissolved oxygen content and turbulence on coastal ocean epibenthic faunal migrations and community associations (Matabos et al., 2012, 2015; Chu and Tunnicliffe, 2015; Gasbarro et al., 2019), and have evaluated redox-dependent biogeochemical processes (Juniper and Brinkhurst, 1986) and the impacts of groundfish activity on sediment resuspension and opal dissolution (Katz et al., 2009). Here, new monitoring provides further insight into exchanges between the seafloor and the water column.

EC measurements have been made from benthic platforms and observatories to assess turbulent momentum and heat fluxes in a number of bottom boundary layer studies (Shaw and Trowbridge, 2001; Walter et al., 2014; Davis and Monismith, 2011). However, the method has not been demonstrated for extended oxygen flux determinations (i.e., >7 days) due to limits of battery power, data storage or sensor lifetimes (Attard et al., 2014; McGinnis et al., 2014; Long et al., 2015). The benthic oxygen flux EC method was pioneered by Berg et al. (2003) and has unique utility for documenting both temporal and spatial variations in rates of benthic primary production and/or respiration (Berg et al. 2003, 2013; Attard et al., 2014, 2019; Rheuban et al., 2014; Glud et al., 2016; Reimers et al., 2016). In practice, the EC method combines high frequency measurements of flow velocity (made with an Acoustic Doppler Velocimeter [ADV] in 3 dimensions) and scalar properties such as oxygen concentrations, temperature or salinity (made with fast-responding sensors) in a fixed sampling volume typically 5–30 cm above the seabed (Berg et al., 2007; Crusius et al., 2008). Using these measurements, fluxes may be resolved at sub-hourly time scales, and they may be assessed in habitats with soft and hard substrates, over a larger benthic footprint than other traditional benthic flux measurement methods. However, one critical caveat of the method is that conditions in the bottom boundary layer must be at least quasi steady-state and moderately turbulent for EC flux derivations to equate to reliable seafloor source or sink estimates (Brand et al., 2008; Holtappels et al., 2013). A unique accomplishment of this study is that measurements necessary to derive both turbulence measures and oxygen and heat EC fluxes were recovered over 222 days. This allowed a systematic and discriminating screening of when conditions were favorable for benthic flux determinations.

2. Materials and methods

2.1. Study site

Ocean Networks Canada has maintained the VENUS observatory node on the east side of Saanich Inlet, outside Patricia Bay, at 100 m depth, since 2006 (Dewey et al., 2007). Saanich Inlet is a semi-enclosed, highly stratified fjord within the Salish Sea on the southern end of Vancouver Island, British Columbia, with a maximum depth of about 240 m and a broad ~70-m sill. Rates of primary production have been estimated as ~38–40 mol C $m^{-2}y^{-1}$ in Saanich Inlet and appear dependent on nutrient sources from the Strait of Georgia (Grundle et al., 2009). Sediment accumulation rates in the deepest sections of the basin range from 0.093 to 0.27 g cm^{-2} y^{-1} and are highest near the northern sill of the basin (Matsumoto and Wong, 1977). The Patricia Bay node is connected to a shore station by a 3-km long fiberoptic Ethernet marine cable. Dissolved oxygen, temperature and salinity are measured nearly continuously by observatory instruments, and these time series display an annual pattern of moderate hypoxia in spring and summer, severe hypoxia in much of the fall, and renewed oxygen levels in winter (Matabos et al., 2012; Gasbarro et al., 2019). Associated with these cycles are movements of epifauna that have been linked to localized episodes of sediment resuspension and changes in the depth of diurnal migrations of zooplankton (Yahel et al., 2008; Matabos et al., 2012). The sediments are fine-grained with organic carbon and nitrogen contents ranging from 1 to 3.5% and from 0.15 to 0.45%, respectively. During severe hypoxic conditions, a surface mat of filamentous sulfur bacteria will commonly form at the sediment-water interface (Yahel et al., 2008; Matabos et al., 2012).

Estuarine circulation is weak throughout most of Saanich Inlet, but intermittent advective exchange has been described as forced by the effects of strong spring-tidal mixing outside the inlet on vertical density gradients across the sill (Gargett et al., 2003; Hamme et al., 2015). In addition, subtidal flow at mid-depths can reverse with the spring/neap tidal cycle, and this oscillation may produce internal waves at the sill with bursts of energy propagating into the main basin (Kunze et al., 2006; Sato et al., 2014). Turbulent dissipation rates in the water column at the study site have been typified as generally low, between ~10^{-9} and ~10^{-8} W kg^{-1} (m^2s^{-3}) based on shear probe microstructure profiles (Rousseau et al., 2010) and Acoustic Doppler Current Profiler (ADCP) and ADV measurements (Sato et al., 2014). Variations in turbulence within the bottom boundary layer in different seasons had not been assessed prior to this study.

2.2. Instrumentation

The central instrument utilized was a Nortek™, Vector, Acoustic Doppler Velocimeter (SN 4868; henceforward referred to as the "Vector") with fixed head, pressure sensor, and an end bell fitted with an internal wiring harness and two connectors, one (8 pin) to accept power from and send data to an external source/controller, and the other (5 pin) to sample analog signals from oxygen and temperature EC sensors (described below). To interface the Vector with the VENUS observatory, 10 m of cabling was run from the 8-pin connector to a custom 24/12 VDC converter and noise filter connected to a secondary observatory 24V junction box called a Science Instrument Interface Module (SIIM), using a wet-mateable Seacon XSL connector. The SIIM unit was mounted on a frame (previously built to support a camera system) and connected by a separate cable to the primary Saanich Inlet node at 100 m depth. An aluminum "birdcage" frame painted with marine epoxy paint, 1.5 m high x 1.0 wide, and open near the base so not to impede flow above the seafloor, supported the Vector in a vertical, head-down orientation.

In deployment, the birdcage frame was attached to the VENUS "camera frame" and both were lowered by wire to the seafloor and released using an acoustic release. After deployment, a Remote Operated Vehicle (ROV) connected the SIIM to the node and carried the birdcage to a position (latitude 48° 39.05676′N, longitude 123° 29.24010′W) on the seafloor ~6 m away from the camera frame (Fig. 1a&b). A CTD (SeaBird 16plus, SN 7128) with SBE-43 oxygen sensor in a flow-through cell with standard SeaBird anti-foulant cartridge was mounted on the camera frame to collect environmental data for comparison to the EC sensors. The inlet of the flow-through cell was 58 cm above the seafloor.

The oxygen and temperature sensors, utilized for EC, extended from and collected measurements through separate "MicroSquid" sensor electronics units developed by Rockland Scientific (Victoria BC). Each MicroSquid received power from the Vector and returned high resolution analog signals from the sensors via a Y-split cable. The electronics in these units are galvanically isolated using optical signal couplers, and the Delrin housings (outer diameter = 5.7 cm, inner diameter = 4.2 cm, 24 cm long) have internal copper cladding and electric chokes to shield against radio frequency noise emitted by the acoustic current meter. Extra shielding connected to the analog ground also extends to the probe holders. The output signals from the instruments are sampled at a rate of 1024 Hz and the full-range of input is 0–5.12V with a 16-bit analog to digital converter. Sensor signals are deliberately over sampled to reduce quantization noise.

The oxygen sensor used was a galvanic microelectrode (supplied by AMT, Rostock, Germany) with linear analog output (0–5 VDC), 12 VDC input, a removable titanium guard, and manufacturer reported 90% response times and lifetimes of 0.2 s and 9–18 months, respectively. In Fig. 1c, the tip of an AMT microelectrode is shown without guard to the

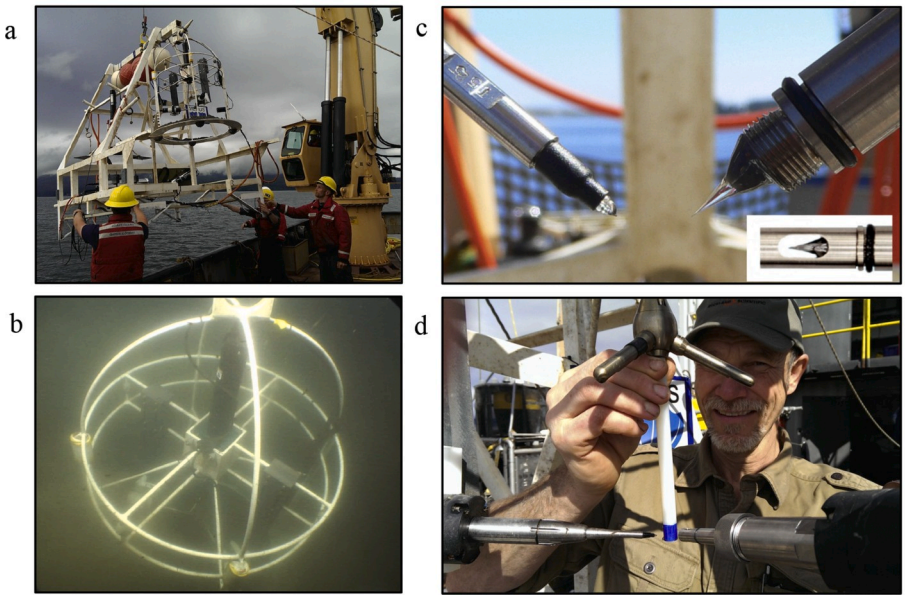

Fig. 1. Images of (a) the VENUS camera frame supporting the EC instrumentation during deployment, (b) the EC "birdcage" on the seafloor apart from the camera frame in the turbid waters of Saanich Inlet, (c) thermistor and galvanic microelectrode tips in an initial configuration without the protective guard for the oxygen sensor (inset), (d) positioning of the MS-T and MS-DO sensors relative to the Vector sampling volume before the May 23, 2013 re-deployment.

right of the tip of the temperature sensor. (The design of the guard is illustrated in the inset image of Fig. 1c.) The temperature sensor was a micro-thermistor (FP07) supplied by Rockland Scientific with signal-plus-signal derivative analog output and a manufacturer reported time constant of 0.007 s. Fig. 1c shows an initial configuration tried with the sensor tips pointing at 45° angles from horizontal and positioned adjacent to the Vector sampling volume. The sensors were deployed within Saanich Inlet in this configuration on May 7, 2013, but the unguarded AMT microelectrode was broken within hours. This loss necessitated an ROV-assisted recovery and redeployment of the "birdcage" frame to the same seafloor position on May 23, 2013. For this second deployment the AMT sensor guard was placed over a new sensor and oriented with an enlarged set of flow-through holes top to bottom to maximize detection of signals associated with vertical velocity variations. The angles from horizontal of the sensors and their backing MicroSquid units were also lowered to ~10° and set 120° opposing (±60° from the +X-coordinate), with sensor tips pulled back ~1–2 cm from the Vector's sampling volume (as shown in Fig. 1d). This change was made to assure no physical interference of the sensors with the acoustic backscatter return beams of the Vector (see Berg et al. 2016 for further discussion of these interferences). From henceforth we will refer to the MicroSquid supported sensors as the "MS-DO" and "MS-T" components of the EC system.

Once deployed, Vector settings were controlled through the observatory using an interface layer, developed by ONC, called a driver. These drivers are developed for each instrument. They pull configuration information out of a database, format commands into instrument specific protocols, establish communications with the instrument, send and receive commands, start the sampling, and then log the time-stamped data in a HEX file, so that all information to and from the instrument is captured and stored. The log files cannot be queried in real time. These log files are closed off at the end of each day, midnight UTC, and can be queried after they are stored in the archive. The Vector settings utilized are listed in Table 1. Time-series data were collected in 30-min bursts at 32 Hz. The velocimeter's sampling volume was ~16 cm above the seabed, as confirmed by return echoes in probe check files.

Table 1
The settings of the Vector used in this study.

Setup	Selection
Sampling rate	32 Hz
Nominal velocity range	0.1 m s^{-1}
Burst interval	1800 s
Samples per burst	56640
Sampling volume	14.9 mm
Transmit length	4.0 mm
Receive length	0.01 m
Analog inputs 1 and 2	FAST
Power output	ENABLED
Powerlevel	HIGH
Coordinate system	XYZ

2.3. Data processing

The daily data files transferred from the Vector were imported into MATLAB routines that were used to parse measurements and instrument information into structure arrays reporting configuration, metadata, units, and data fields. These files were typically 120 MB in size and included all system and probe check data routinely produced by Nortek Vector instrument software. Further processing started with these individual files and included MATLAB code functions that converted raw MS-T and MS-DO readings to outputs in units of °C and μmol L^{-1} (at in situ conditions). The thermistor calibration coefficients were provided by Rockland Scientific, but the oxygen sensor's output was calculated from a calibration configuration file based on (1) pre-deployment readings in deoxygenated and air-saturated water (to give a linear voltage to partial pressure calibration function) and (2) solubility changes in situ as a function of salinity, pressure and MS-T temperature. Time-series of temperature, dissolved oxygen and velocities in XYZ coordinates (denoted henceforth as *u, v, w*) were also routinely filtered to remove spikes (extreme data outliers) using a phase-space method adapted from Goring and Nikora (2002) whereby spikes are replaced with points based on a spline fit to adjacent data. These "cleaned" time series, together with coincident pressure measurements and burst number identifiers, were then saved in arrays that were reduced from 32 to 8 Hz by computing sequential four-point averages. All of these methods are common practice in the early stages of EC data processing (Lorrai et al., 2010; Reimers et al., 2012). Later stages included assessments of the impacts of alternate detrending methods and velocity coordinate system rotation methods on EC fluxes, and on derivations of

power density spectra, turbulent kinetic energy (TKE), and turbulence dissipation (ε).

The final approach chosen to separate fluctuating components from a time-dependent mean was to detrend all data with a 0.005 Hz high-pass frequency filter (i.e., trends of frequencies less than 0.005 subtracted when computing variances, see Reimers et al., 2012), without any co-ordinate rotation. Fig. 2 illustrates typical signal variability and variance preserving spectra produced with this approach. Justification for these choices stems from: (1) a desire to attenuate flux contributions due to low frequency advective oscillations within the temperature and oxygen time series, (2) the recorded pitch and roll angles of the Vector were constant at −3.0° and −13.8°, respectively, reflecting the slope of the seafloor, and (3) an observation that two-angle and planar fit rotation approaches (described for example in Lorke et al., 2013) can misrepresent the local streamline under weak flows, and in this study often produced greater variance in vertical velocities by burst and unrealistic angle adjustments for the Z coordinate. For each 30-min 8-Hz data burst, using the same procedures for separating fluctuations as for EC fluxes, TKE was assessed as TKE $= \frac{1}{2}(\overline{u'u'} + \overline{v'v'} + \overline{w'w'})$. Dissipation was estimated from a one-dimensional spectral equation of vertical velocity fluctuations (Shaw et al., 2001):

$$S_{ww}(k) = \frac{9}{55}\left(\frac{4 - cos\theta}{3}\right)\alpha\varepsilon^{\frac{2}{3}}k^{-\frac{5}{3}} \quad (1)$$

following the approach of Reidenbach et al. (2006) that first removes any noise floor at frequencies ≥ 1 from the spectrum. In equation (1), S_{ww} (k) is the power spectral density as a function of the wave number k; $\theta = 90°$ is the angle from the direction of mean flow; and $\alpha = 1.56$ is the empirical Kolmogorov constant for velocity. Wave number space was converted to frequency space as: $f = \frac{Uk}{2\pi}$ where U was computed as the mean of the current speed $c=(u^2 + v^2 + w^2)^{0.5}$ over the burst. U values were also used in Reynolds number calculations.

Finally, we also introduced time lag adjustments (up to ± 4 s and independent for each sensor and burst) to maximize cross-correlations between the fluctuations in temperature (T') and w', and dissolved oxygen (C') and w' when computing EC fluxes as $\overline{w'T'}\mathbb{C}_p\rho_w$ and $\overline{w'C'}$, respectively. The added terms for the heat flux are $\mathbb{C}_p$ the specific heat of the bottom seawater (J g^{-1} $^oC^{-1}$), and ρ_w the seawater density (g cm^{-3}) (Crusius et al., 2008). We applied J $cm^{-2}s = 10^4$ W m^{-2}.

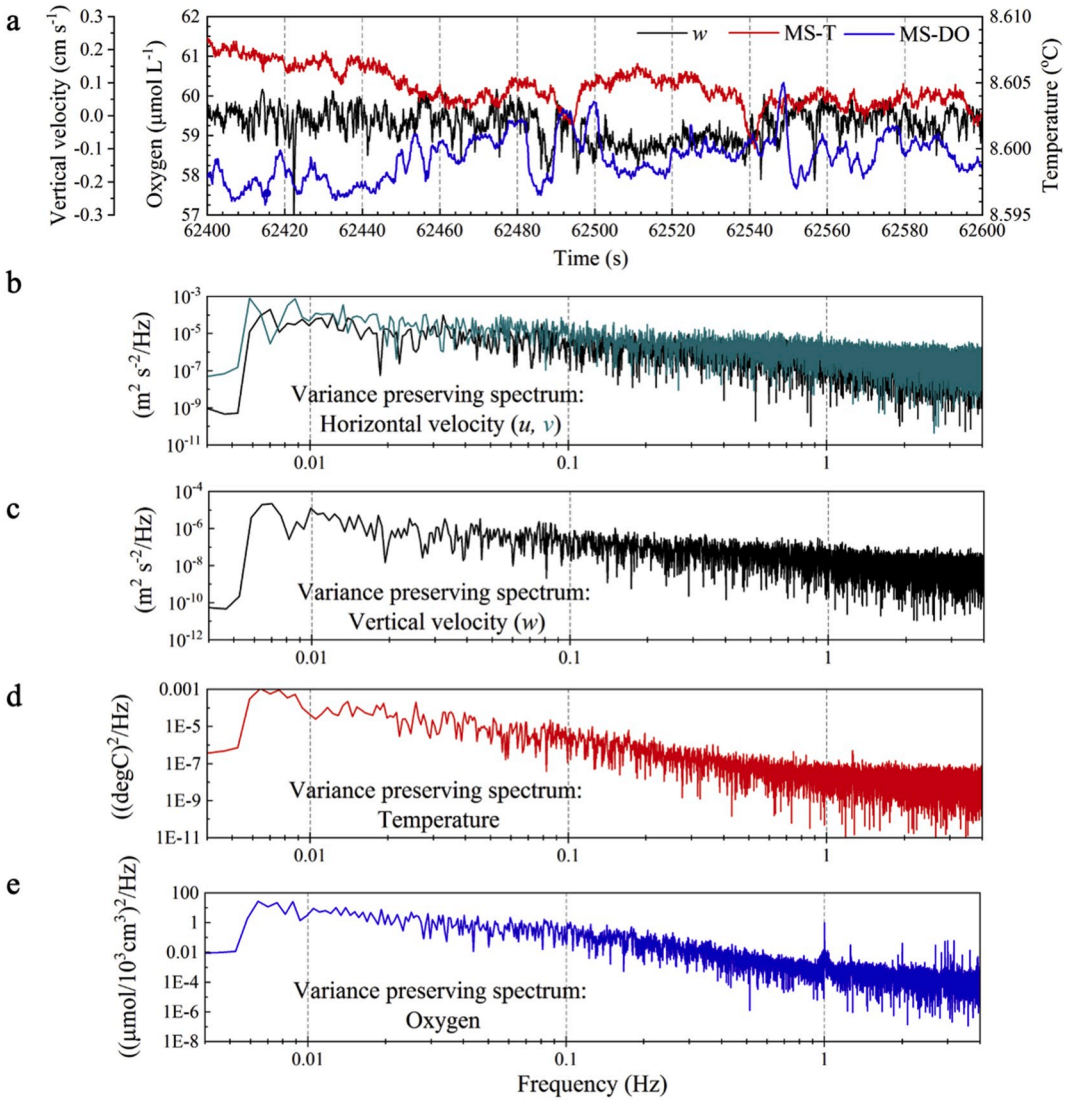

Fig. 2. Variances in EC sensor measurements portrayed as (a) a 200-s time-series, and (b–e) variance preserving spectra. These measurements were recorded May 28, 2013.

3. Results

3.1. Sensor measurements and flow characterizations

The Vector, MS-T, and MS-DO were operated as an integrated EC system for 284 days, through the VENUS Observatory, at a position ~6 m away and downslope from the independent camera frame-mounted CTD and SBE-43 oxygen sensor. Fig. 3a–d illustrates environmental conditions recorded by the CTD sensors over the complete duration of the deployment together with near-seabed flow speeds derived from the Vector. Fig. 3e focuses in on two periods of decreasing dissolved oxygen for later discussion of factors affecting rates of oxygen decline in the bottom boundary layer. To demonstrate the quality of the MS sensor measurements and additional environmental information captured by the Vector, Figs. 4–6 compare 8-Hz EC sensor records to measurements from the CTD (panels b and c), and display derived flow and turbulence parameters (panels d and e) and EC fluxes (panel f) for each 30-min burst from three differing 3-day records. These were collected: (1) during spring intermittently hypoxic conditions and during a spring tide, soon after deployment, May 27–29, 2013 (Fig. 4), (2) during fall under constant hypoxia and a neap tide, October 1–3, 2013 (Fig. 5), and (3) during early winter conditions coincident with initial stages of bottom water renewal and a spring tide, December 29–31, 2013 (Fig. 6). Fig. 6 also shows the last three days with complete MS-DO measurements before the galvanic oxygen microelectrode was broken on January 1, 2014, probably by a fish strike. Thus, the length of the record that included all sensors was limited to 222 days.

The MS-T and MS-DO time-series as displayed in Figs. 4–6 suggest consistent and sustained sensor responses to multi-frequency temperature and dissolved oxygen variations as well as offsets in running means from the CTD sensors that either reflect the spatial separation of sensors or small calibration errors. Specifically, the EC sensors were closer to the seafloor and deeper in the water-column (recorded pressures were higher by ~ 1.6 dbar) than those on the CTD, and the EC sensors usually reported lower concentrations of dissolved oxygen and slightly higher temperatures (Figs. 4–6, panels b and c). The thermocline structure of Saanich Inlet is unique and follows a seasonal progression whereby in winter and spring, deep waters are warmer than the surface, but this pattern weakens and reverses in summer and fall (Anderson and Devol, 1973; Timothy and Soon, 2001). Consequently, correlations between temperature and dissolved oxygen are negative in the time series from May and December (Figs. 4 and 6) but intermittently positive in October when the ranges of variations were also small (Fig. 5) (Supplemental Fig. 1). Abrupt transitions with signatures of seiching and internal wave displacements, seen for example in Fig. 4 at hour 24, or Fig. 6 at hour 35, illustrate these T-DO relationships most clearly. Artificial oxygen variations caused by velocity effects (Holtappels et al., 2015) were not evident in DO-velocity component relationships (Supplemental Fig. 2a&b), nor did the sensitivity of any of the sensors appear to change over time, which may have been benefits of the generally narrow range of flow speeds and little biofouling under hypoxia. In the 3-day example records, the May record displays the highest and most variable

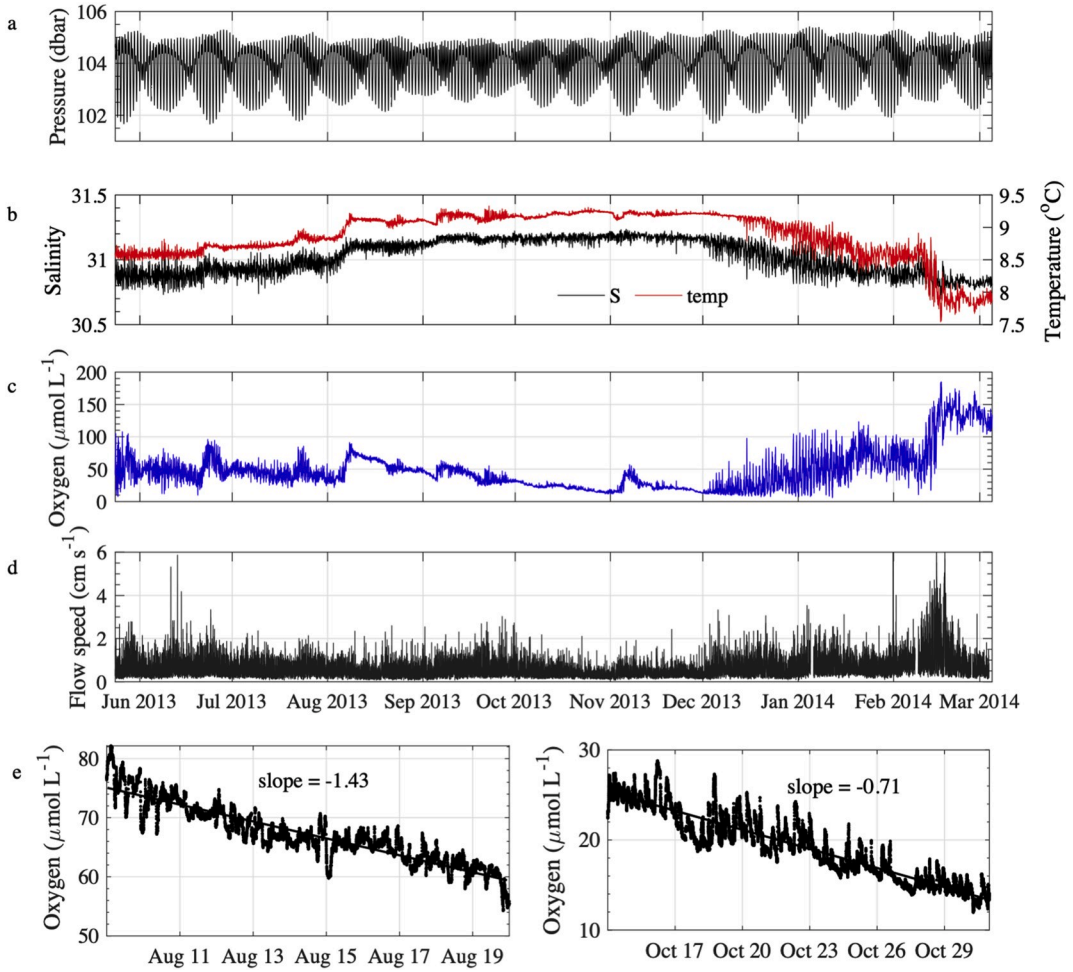

Fig. 3. (a–c) Sensor records from CTD instrumentation mounted on the VENUS camera-frame platform and (d) the EC system Vector. All measurements were reduced to 1-min averages and displayed as line plots. No Vector data is shown for January 5, 2014 and February 8, 2014 due to missing or corrupted files. (e) Illustrative intervals of declining dissolved oxygen concentration.

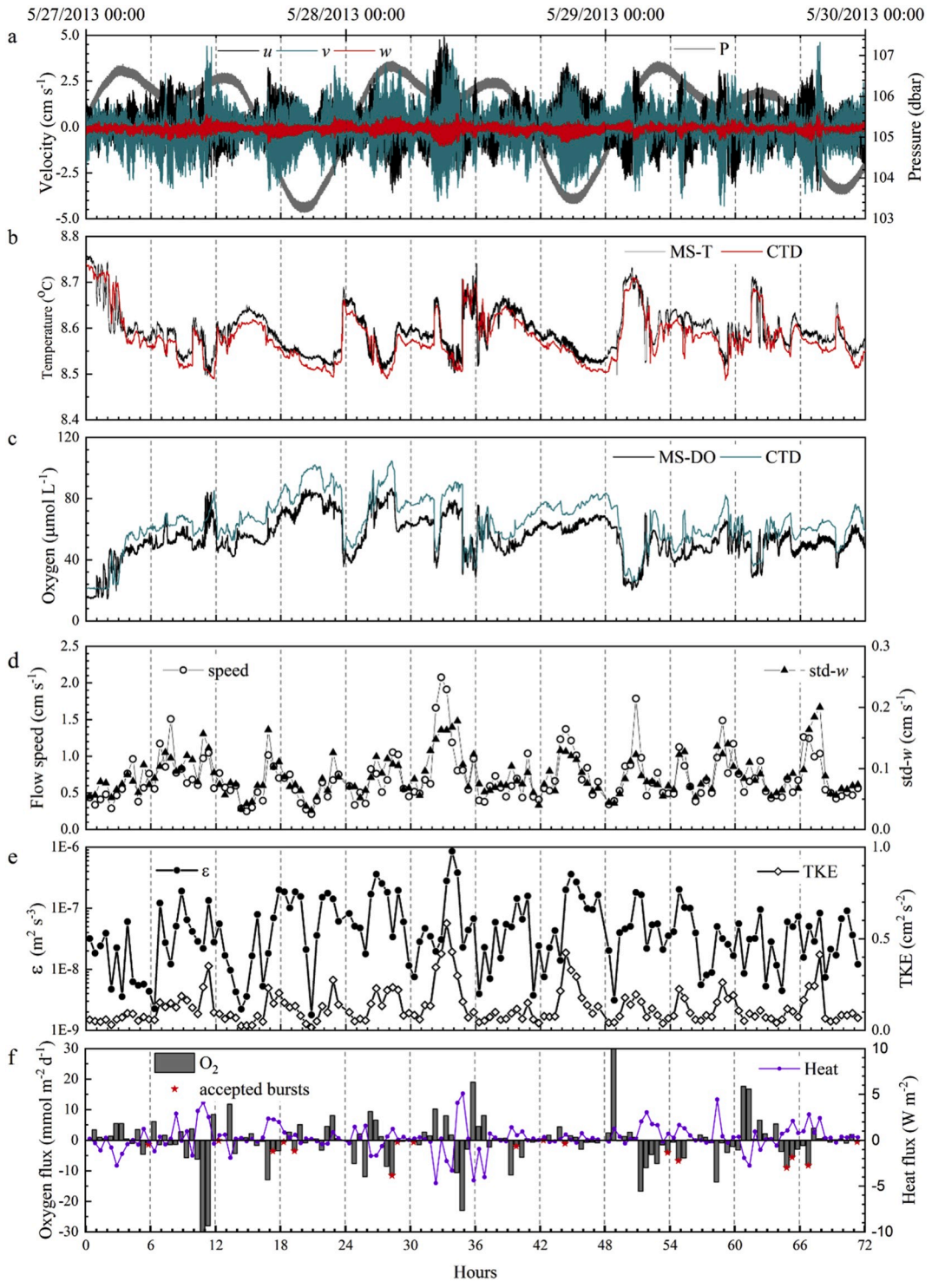

Fig. 4. Three days of EC sensor data from early in the deployment (May 27–29, 2013 UTC) with (a) three velocity components and pressure reported at 8 Hz, (b) MS-T (8 Hz) compared to neighboring camera frame CTD temperatures (1-min averages), (c) MS-DO (8 Hz) versus CTD-SBE 43 oxygen concentration measurements (1-min averages), (d) 30-min burst averages of flow speed and std-*w*, (e) turbulence parameters TKE and ε, and (f) EC fluxes. Within this 3-day series there were 17 bursts accepted for EC flux derivations under criteria explained in the text. These are marked with red stars. (For interpretation of the references to colour in this figure legend, the reader is referred to the Web version of this article.)

velocities, and the October record displays the most quiescent and stable bottom boundary layer conditions. In analyses by burst, TKE assessments follow trends in flow speed and std-*w*, but dissipation rates of turbulence, ε, vary over 3 orders of magnitude with the highest values in the May record (Fig. 4e).

To further characterize the incidence of energetic flows at the study site, we grouped the 1-min averages of current speed $\bar{c}$ displayed in Fig. 3 by month and then computed monthly distributions by percent occurrence in the fully observed months of June through February (Table 2). A threshold of initial interest was mean flow speeds greater than 2 cm s^{-1}, which was surmised by Brand et al. (2008) in a study of Lake Alpnach in central Switzerland, as necessary to produce sufficient

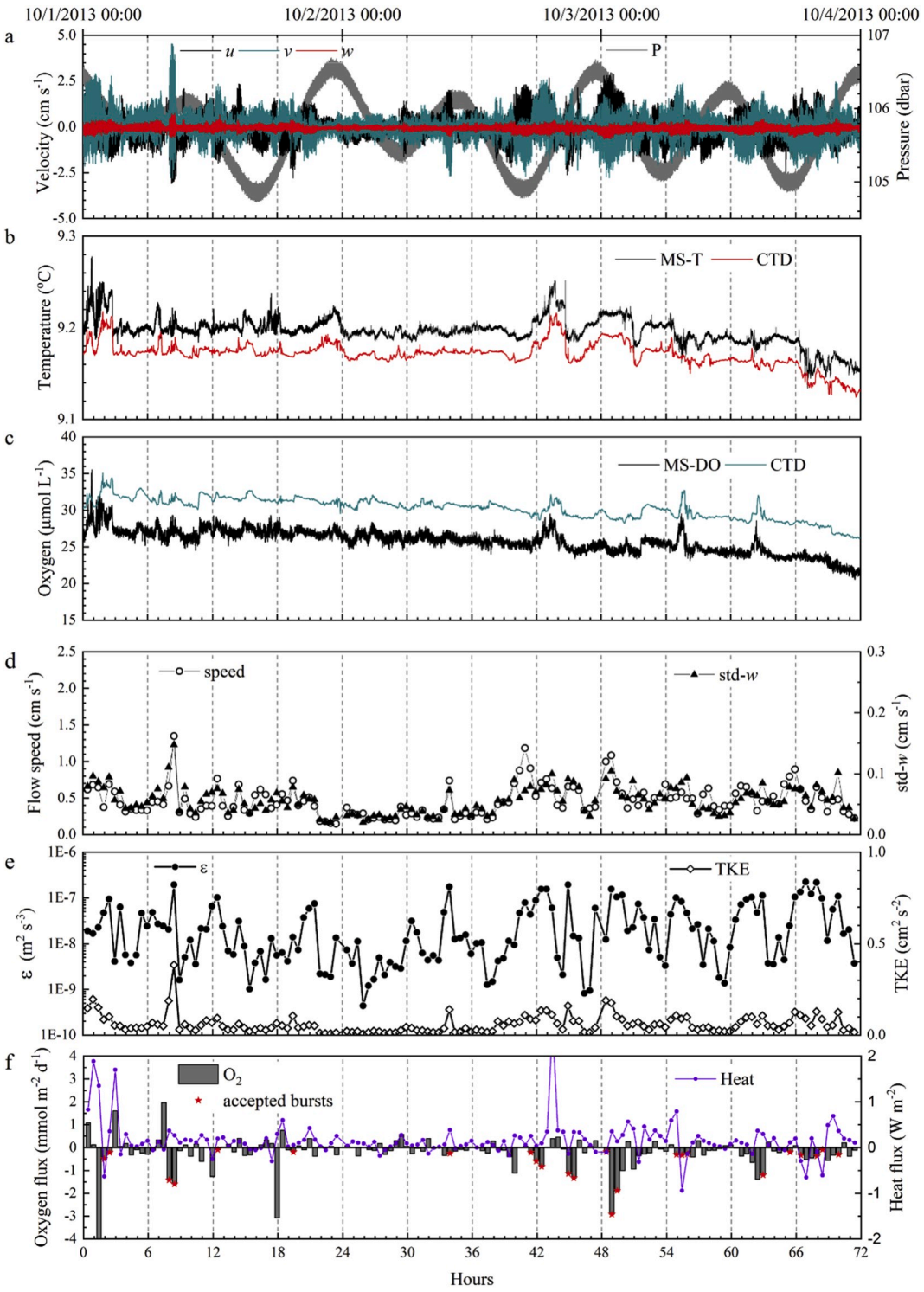

Fig. 5. Three days of EC sensor data during severe hypoxic conditions (October 1–3, 2013 UTC). Panels a–f display the same parameters as in Fig. 4 with scales adjusted to the observed ranges. Within this 3-day series there were 25 bursts accepted for EC flux derivations.

turbulence to overcome viscous forces and transport oxygen through a stratified benthic boundary layer. In the Lake Alpnach study, the 2 cm s^{-1} velocity threshold also corresponded to a Reynolds Number (Re) ~1700 (where $Re = L\bar{c}/\nu$; L is the characteristic length scale $= z_{meas}$, and ν is the kinematic viscosity). This critical Re value would have been met instead by a mean current ~1.5 cm s^{-1} in Saanich Inlet given that z_{meas} = 16 cm. Even this lower velocity threshold was rarely observed at the study site (Table 2). However, current speeds computed for each 30-min burst within the time series in Figs. 4–6 (panels d) do show that sub tidally modulated peaks in flow were common in daily records. Furthermore, the magnitude of the standard deviation of the vertical velocity (std-w) follows the magnitude of current speed. Brand et al. (2008) had observed that std-w needed to be at least 0.1 cm s^{-1} to detect significant eddy fluxes in Lake Alpnach. Berg et al. (2009) suggests instead that the EC technique can give valid benthic flux estimates when std-w values are as small as 0.078 cm s^{-1} as long as mean currents $\geq$ 1 cm s^{-1}. The Berg et al. (2009) study considered EC measurements made 10 cm above the seafloor at a 1450 m-deep site in Sagami Bay, Japan;

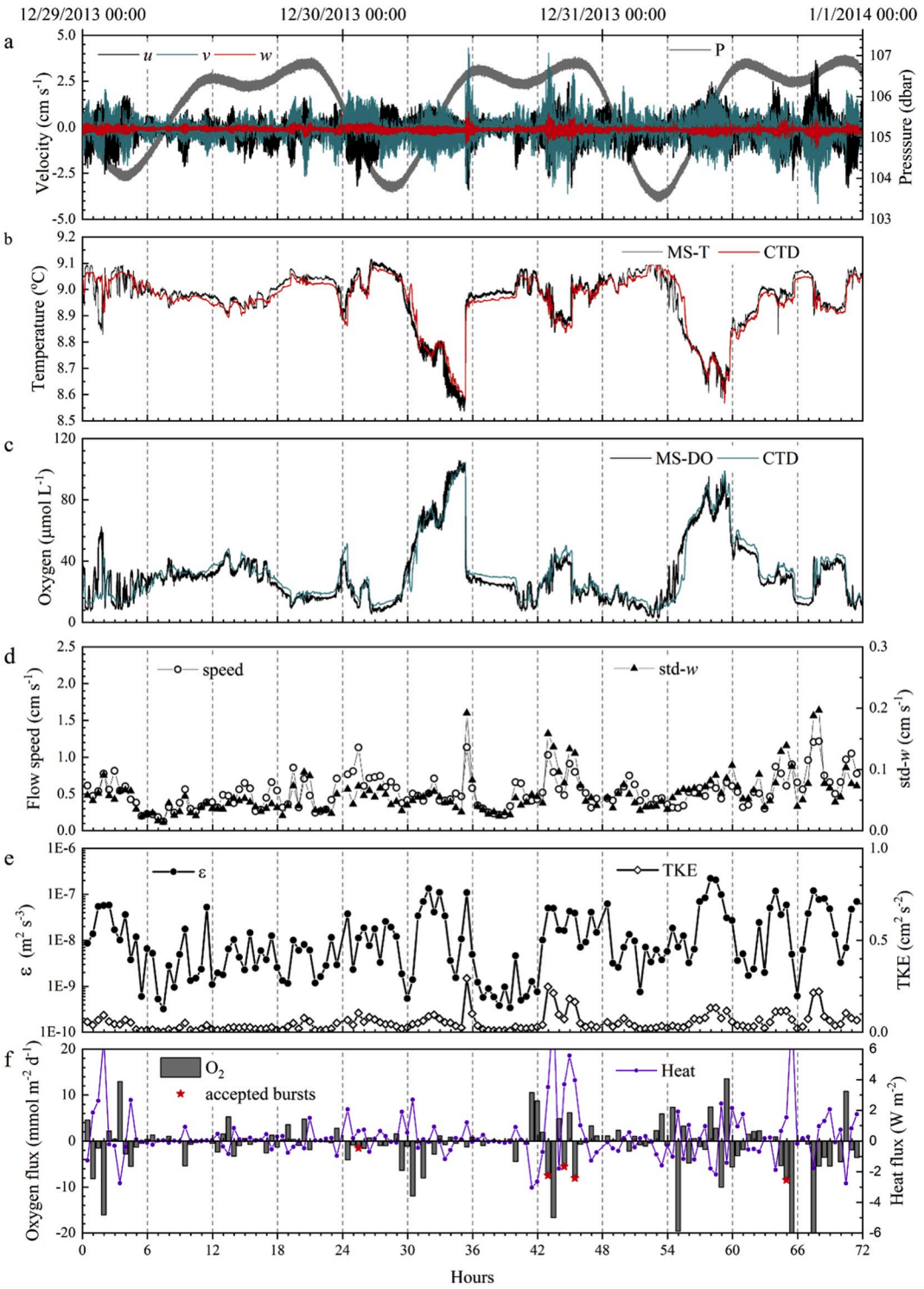

Fig. 6. EC sensor data from December 29–31, 2013 UTC. Panels a–f report the same parameters as in Figs. 4 and 5. Within this 3-day series there were 5 bursts accepted for EC flux derivations.

thus, suggesting a corresponding Re threshold ~ 600.

3.2. Benthic flux derivations

Transient water mass displacements created by processes such as seiching and internal waves in a benthic environment will result in EC fluxes that do not reflect seafloor exchange rates. This has been demonstrated through models and by cases studies to be because the seafloor source/sink term is not in a steady state balance with the vertical transport of properties by turbulent eddies (Holtappels et al., 2013; Lorke et al., 2013). EC fluxes may also underestimate benthic exchange rates when turbulence is too weak to mix scalar properties fully between the boundaries of the bottom boundary layer (Brand et al., 2008).

Faced with a benthic environment with periods of weak turbulence and variable water mass displacements, the solution developed here was to apply criteria to eliminate bursts occurring when the bottom boundary layer was not adequately turbulent or when transient shifts in

Table 2
Flow speeds observed 16 cm above the bed throughout the deployment. Distributions of % occurrence are based on monthly compilations of 1-min averages of Vector data collected at 32 Hz.

Month	0–0.5 cm s^{-1} (%)	>0.5–1.0 cm s^{-1} (%)	>1.0–1.5 cm s^{-1} (%)	>1.5–2 cm s^{-1} (%)	>2 cm s^{-1} (%)	Mean ± sd (cm s^{-1})
Jun 2013	45.5	43.6	8.6	1.7	0.6	0.61 ± 0.34
Jul 2013	51.6	43.6	4.5	0.3	0.02	0.54 ± 0.24
Aug 2013	67.7	30.0	2.0	0.2	0.04	0.45 ± 0.22
Sep 2013	50.0	41.5	7.1	1.1	0.3	0.57 ± 0.30
Oct 2013	78.5	19.8	1.6	0.1	0.02	0.40 ± 0.20
Nov 2013	81.3	17.8	0.8	0.1	<0.01	0.38 ± 0.17
Dec 2013	47.3	43.3	7.4	1.5	0.4	0.59 ± 0.32
Jan 2014	32.0	55.75	10.3	1.4	0.5	0.67 ± 0.31
Feb 2014	19.5	46.5	19.8	6.8	7.4	0.98 ± 0.66

bottom water properties were observed. Up to the day the MS-DO sensor failed, acceptable bursts were required to display mean values of TKE >0.06 cm^2 s^{-2}, and std-w > 0.07 cm s^{-1} (thereby giving slightly more leeway for low turbulence than recommended in earlier studies). Furthermore, interquartile range values of T and C were derived for each burst, and it was required that $iqrT \leq 0.025$ °C, $iqrC \leq 4$ μmol L^{-1} to screen out bursts with temperature and DO values exhibiting wide statistical dispersion due to transient shifts in bottom water properties. These values had to be tuned to retain what appeared as the turbulence-driven variances in the data and may not be optimal for other environments with different dynamics or greater fluxes. Thresholds for flow speed and ε were not specifically imposed because these parameters correlated with the parameters chosen (see for examples Figs. 4–6) and did not provide unique screening. Two final conditions were to exclude bursts when $\overline{w'C'} > 0$ (unrealistic if conditions were at steady-state) or the mean flow direction came from directly behind either the MS-T or MS-DO sensors (±50–70° relative to + X). Table 3 summarizes all six screening criteria. The fluxes associated with acceptable bursts (n = 670) were separated by day, and averages of these fluxes compared to daily averages of all bursts (Fig. 7). As anticipated this comparison demonstrates the accepted bursts often yielded fluxes higher in magnitude than those assessed without turbulent transport criteria.

Lastly, temporal trends in heat and oxygen fluxes were prepared from weighted averages representing 5-day windows, and these are displayed with trends in bottom water properties and turbulence in Fig. 8. The percentage of the record accepted for deriving realistic seafloor exchange rates in each 5-day window ranged from 0.4 to 17% (Fig. 8c). No single screening criteria uniquely disqualified all bursts, but the TKE and std-w thresholds were restrictive most often due to low turbulence levels (illustrated with the 5-pt moving average of daily means in TKE in Fig. 8b). The benthic oxygen uptake rate average (±1 standard deviation) based on the 5-day averages in Fig. 8a was −1.6 ± 1.2 mmol m^{-2} d^{-1} (range −0.06 to −6.21). The heat flux averaged 0.27 ± 0.57 W m^{-2} (range −0.94 to +2.67).

Table 3
Criteria applied to distinguish bursts of EC measurements acceptable for derivations of benthic exchange rates.

Criterion	Basis
Standard deviation w > 0.07 cm s^{-1}	Adequate turbulence
TKE >0.06 cm^2 s^{-2}	Adequate turbulence
Interquartile range C < 4 μmol L^{-1}	Minimal advection; steady state bottom boundary layer conditions
Interquartile range T < 0.025 °C	Minimal advection; steady state bottom boundary layer conditions
$\overline{w'C'} > 0$	Oxygen flux realism under steady state conditions in an environment at 100 m water depth
Flow direction not (±50–70° relative to + X)	No flow interference stemming from flow from behind MS-DO or MS-T sensors

4. Discussion

At the VENUS observatory site, low turbulence and extended periods of hypoxia with little change in temperature were observed to contribute to low overall rates of sediment oxygen uptake and heat exchange derived by EC after applying criteria for the acceptance of fluxes as in balance with a seafloor sink or source. Presumably, these exchange rates were constrained largely by diffusion and conduction (1) across a changeable, mm-scale, diffusive/conductive boundary layer and (2) within the surface sediments, where in the case of oxygen the oxidation of anaerobic by-products and/or aerobic respiration are responsible for the oxygen demand (Jørgensen and Boudreau, 2001). In other similar settings, in situ microprofiling and flux chamber techniques have been executed to characterize rates and controls of oxygen uptake and have shown that there is extensive small-scale variability in oxygen microprofiles and a sensitivity of diffusive fluxes to dynamic forcing (Glud et al., 2009; Bryant et al., 2010). There have been no in situ measurements by these alternative methods at the observatory site, but one study, in which cores (collected in February 2006) were incubated ex situ, showed that in an "undisturbed state" the oxygen uptake rate averaged ~ −0.45 mmol m^{-2} d^{-1} (Yahel et al., 2008). However, this same study reported uptake rates increased abruptly to ~ −1.6 mmol m^{-2} d^{-1} when resuspension mimicking flatfish activity impacted the deposits. Another study based on core samples taken in July 2011 and September 2013 reports oxygen uptake rates of −13.7 ± 9.3 mmol m^{-2} d^{-1} (n = 7) and oxygen penetration depths into the sediments of 3.7–4.7 mm (Belley et al., 2016). We caution that the cores in the latter study were not at steady state due to deliberate aeration of the overlying water at the onset of ex situ incubations. Nonetheless, oxygen uptake rates of similar magnitude may occur during annual periods of peak oxygenation of the lower water column (usually during March and April), i.e. during months when we were unable to collect MS-DO measurements.

For a final comparison to the derived fluxes, we use a predictive relationship $DOU = 2\varnothing\frac{D_s C_w}{L}$ established for marine sediments that relates diffusive oxygen utilization rates (DOU) to the O_2 penetration depth (L), the sediment porosity ($\varnothing$), molecular diffusion coefficient of O_2 in the surface sediment layer (D_s), and bottom water concentration (C_w) (Cai and Sayles, 1996). By this relationship, if $\varnothing = 0.9$ and $L = 4$ mm, DOU would scale with C_w. For a check on the EC fluxes, the relationship predicts DOU would equal −1.8 mmol m^{-2} d^{-1} at a bottom water concentration of 50 μmol L^{-1} (i.e., at a concentration typical in June and July at the VENUS site).

During the severely hypoxic periods within October and November, oxygen fluxes were for weeks <0.5 mmol m^{-2} d^{-1}, and the % of the record meeting our EC acceptance criteria was very low due to nearly uninterrupted low levels of turbulence (Fig. 8). We accept that the EC method was at its limit during this time window and not well suited for determining fluxes. However, even with this qualification, it is significant that there is consistency in flux measurements throughout most of the record and that greater oxygen and heat fluxes are observed at the winter transition when bottom water oxygen concentrations and turbulence started to increase, and temperature was beginning to decline.

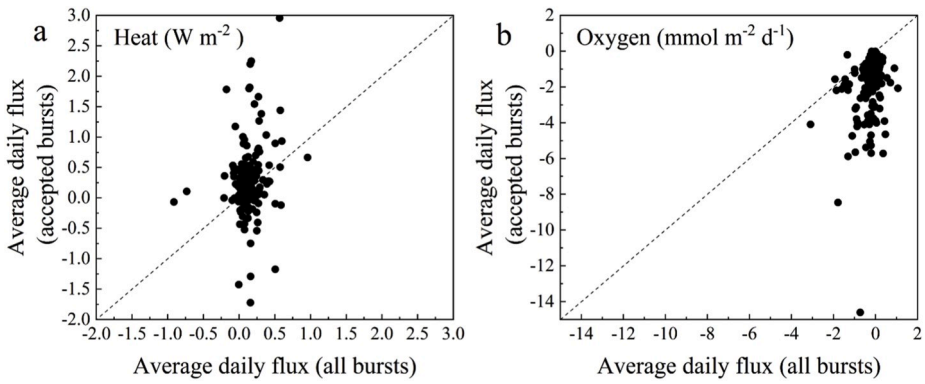

Fig. 7. Comparison of average daily heat and oxygen EC fluxes determined from all versus only the accepted 30-min bursts within a day. Two days with all-burst outliers and 51 days with no accepted bursts are not represented.

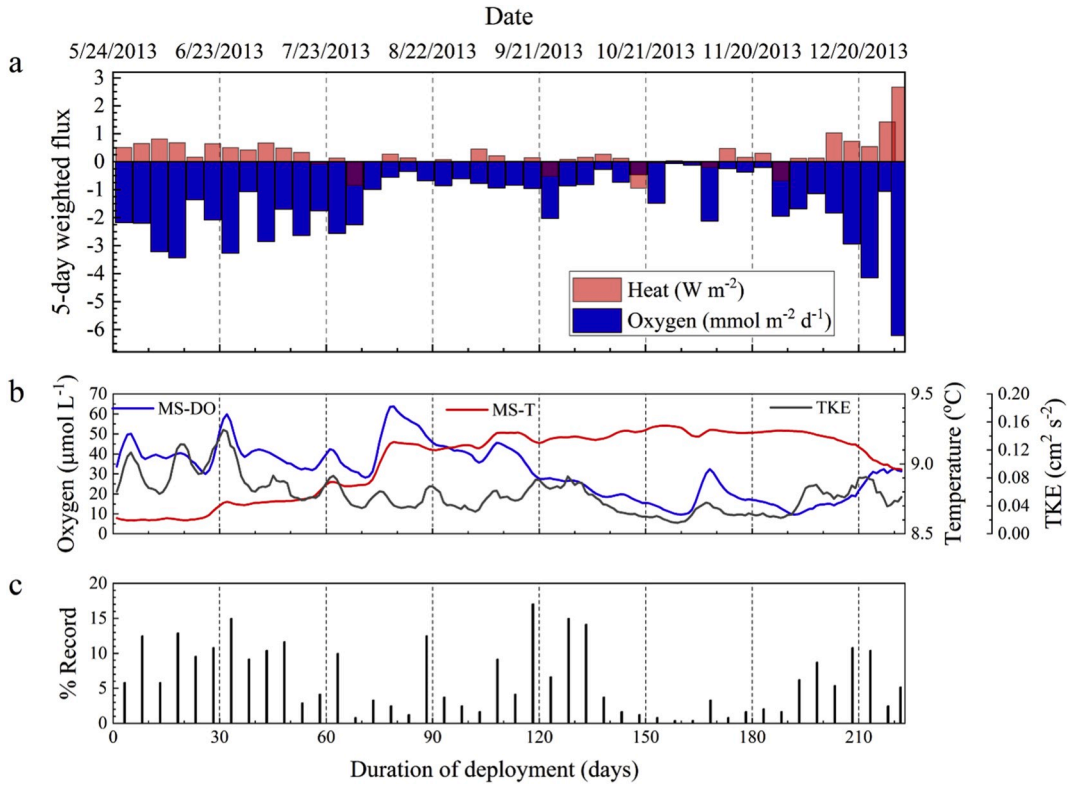

Fig. 8. (a) Averages of accepted fluxes in 5-day blocks (where each accepted burst has equal weight), (b) 5-point moving average of daily mean bottom water conditions of dissolved oxygen, temperature and TKE measured by the EC sensors, and (c) percent of record in each 5-day block meeting criteria for EC fluxes representing benthic exchange rates.

The heat fluxes were generally out of the seabed, bidirectional in summer months, but followed changes in bottom water temperatures. Colder bottom waters trigger heat to be released from sediments that are warmed during summer and that have an underlying geothermal gradient (Stranne and O-Regan, 2015). Assuming a typical thermal conductivity for a high porosity sediment of 0.9 W m^{-1} K^{-1} (Goto and Matsubayashi, 2009), a temperature increase of 0.33 °C across the uppermost 10 cm of sediment could sustain the observed average heat flux. A heat-flux transect across the Cascadia subduction forearc including the continental shelf and Vancouver Island, constrained by borehole measurements and inferences made from the depth to the bottom-simulating reflector (BSR), indicates the marine heat flow expected from the geothermal gradient in this region is approximately 0.04 W m^{-2} (Hyndman and Wang, 1993). Within Saanich Inlet, bottom water warming from July through October may oppose geothermal heat conduction explaining the oscillating heat exchange in summer. Few studies have considered the dynamics of sediment-water heat fluxes except in lakes and shallow marine lagoons where sediment heat transfer can be highly variable and influenced by groundwater discharge (Fang and Stefan, 1996; Smith, 2002; Crusius et al., 2008). A compelling attribute of the EC flux method for any environment is its reflection of wider seafloor footprints than can be characterized by core or benthic chamber incubations, or gradient-based measurements (Berg et al., 2007). Thus, the EC approach has advantages of integrating the spatial variability of the seafloor into fluxes measured over time under changeable conditions. Here observatory-based EC is also shown to be operationally sustainable over more than half a year.

The observed flux record (Fig. 8a) and coupled velocity measurements (Table 2) add new information to ongoing studies of cycles of hypoxia, benthic ecology and turbulence at the VENUS observatory site

in Patricia Bay and in fjords more broadly. Rates of dissolved oxygen depletion in the bottom boundary layer on the order of 1–2 μmol L^{-1} d^{-1} (Fig. 3e) are supportable by benthic fluxes of ~ -1 to −2 mmol $m^{-2}d^{-1}$ only to a height above the seafloor of ~1 m (assuming no other exchanges). This scaling suggests for hypoxic conditions to extend tens of meters into the water column as is the norm in Patricia Bay in summer and fall (Gasbarro et al., 2019), respiration associated with suspended fine particles or dissolved organic matter in the water column must be very active, or more likely that much of the oxygen decline is a result of deeper low-oxygen water being pushed upward and mixed laterally to meet the basin's sloped sides after intermittent renewal events forced by far afield mixing at the channel entrance (Hamme et al., 2015).

Limited benthic oxygen exchange favors anaerobic metabolism in underlying sediments and organic carbon accumulation, making fjords such as Saanich Inlet high spots for organic carbon burial even at their margins (Canfield, 1989; Smith et al., 2015). The rates of seabed oxygen consumption derived here are lower than integrated rates of sulfate reduction in Saanich Inlet sediment cores (12–38 mmol m^{-2} d^{-1}; Reeburgh, 1983) indicating that carbon oxidation in sediments is dominated by sulfate reduction processes throughout the basin, and that in the hypoxic zones, seabed oxygen consumption is primarily a result of the oxidation of sulfide and other reduced metabolites. The mats of sulfur oxidizing bacteria that develop in October and November following the settling of spring and summer phytoplankton blooms are consistent with the importance of sulfide oxidation and may fix additional carbon through chemoautotrophy (Juniper and Brinkhurst, 1986; Matabos et al., 2012). October and November are also characterized by low abundances of mobile epifauna, minimal velocities, low turbulence, severe hypoxia, and reduced benthic oxygen fluxes - all interrelated. It has been shown that as ventilation of the bottom boundary layer occurs more frequently between December and January, the shrimp *Spirontocatis sica* and the flatfish *Lyopsetta exilis* return to the seabed in relatively high densities (Matabos et al., 2012) which is coincident with the higher oxygen utilization observed in late December (Fig. 8a). Part of this increase is likely caused by bioturbation and resuspension of the sediment (Yahel et al., 2008; Glud et al., 2016). As the winter progresses, it would be interesting in future work to evaluate to what the extent oxygen fluxes increase further and how carbon turnover is altered. It would also be insightful to quantify the effects of stronger local flows and higher mean turbulence levels on benthic fluxes.

5. Conclusions

This research presented several unique challenges. The first was the choice of an EC oxygen sensor that was fast-responding, long-lasting in the marine environment, and readily calibrated. The MS-DO served this purpose well when deployed with a slotted guard cap over its galvanic microelectrode. This sensor returned reliable results without any recalibration for 222 days before failure, and when it was recovered, it was evident that it had been physically broken, probably by a fish impact. If the guard affected the sensor response-time or flow patterns around the sensor tip, the smallest flux-contributing eddies may have been missed (Fig. 2). One other study that used these sensors for EC measurements under sea ice indicates that the MS-T and MS-DO sensors are able to resolve temperature and oxygen signals carried by eddies ranging up to 10 Hz and 2 Hz, respectively (Else et al., 2015). Other new sensors are being introduced that promise to do the same or better such as the fast-responding dual oxygen-temperature Rinko EC optode (JFE Advantech, Japan) (Berg et al., 2016). This sensor has a 6-mm tip diameter and bulky body, which like the MicroSquid sensors may affect flow when positioned upstream of the prevailing current; but it does offer robustness. Future research needs to be undertaken to look at the flow disturbance effects of these bulky sensors more closely, and perhaps to change aspects of their design and/or how the sensors are connected to their electronics. Measures to prevent biofouling should also be introduced especially when conducting experiments in warm photic waters.

The second challenge was how to best treat the EC results once it became evident that turbulence was generally low and transient conditions common. Other aquatic EC studies have reported eliminating some segments of EC time series because of issues such as sensor response irregularities, low flow speeds, flow through instrument frames, or transient conditions (Berg et al., 2009, 2013; McCann--Grosvenor et al., 2014; McGinnis et al., 2014), but this is the first to use multiple parameters systematically within data processing scripts to identify segments suitable to accept as benthic fluxes. In part this was necessary because of the volumes of data recovered. The number of acceptable bursts was low (overall only 6.3% of the record), but the fluxes derived for acceptable bursts are credible and indicate predictable seasonal patterns (Fig. 8).

The establishment of a global network of ocean observatories is underway with the fundamental goal of understanding the complex interplay of physical, biological, chemical and geological processes operating within the marine environment (Favali and Beranzoli, 2006). Aquatic eddy covariance is a technique that has emerged and matured within the past two decades and is now ready to be implemented more broadly and/or in combination with other approaches to near-bottom flux measurements such as those based on combined rates of turbulent kinetic energy and tracer variance dissipation derived from similar field observations (Bluteau et al., 2018), or based on sampling chemical and velocity gradients in the bottom boundary layer (Holtappels et al., 2011). The fundamental requirements of the EC technique, when it is applied in the bottom boundary layer to evaluate benthic fluxes, are that mean current velocities and mean scalar properties of interest are steady over the interval of time used for a flux assessment and that turbulence is active enough to dominate transport (Lorke et al., 2013). In many coastal environments these conditions are met much more often, and oxygen uptake rates are tens of times higher than observed in Saanich Inlet (Glud, 2008). This points to the uniqueness of the fjord environment, and it teaches us that these coastal basins may best be characterized as regional sediment traps that promote the burial of marine and terrestrial sources of organic matter by restricting oxygen exposure, limiting oxygen demand, and preventing the export of organic matter to outer shelf and slope habitats.

Declaration of competing interest

The authors declare the following financial interests/personal relationships which may be considered as potential competing interests: Mr. Rick Noel is an employee of Rockland Scientific. Instrumentation described in this manuscript was developed at Rockland Scientific and purchased by Oregon State University for this research. Mr. Noel is included as a co-author because he went to extra efforts to assist the project in executing the field experiment.

CRediT authorship contribution statement

Clare E. Reimers: Conceptualization, Formal analysis, Software, Visualization, Writing - original draft, Writing - review & editing, Funding acquisition. **Rhea D. Sanders:** Investigation, Data curation. **Richard Dewey:** Supervision, Resources, Project administration, Writing - review & editing. **Rick Noel:** Resources, Investigation.

Acknowledgements

This research was supported by grants from the M. J. Murdock Charitable Trust and the U.S. National Science Foundation (OCE awards 1061218 and 1634319). We also thank the support of the Canadian Foundation for Innovation and the Province of British Columbia for funds to build and operate Ocean Networks Canada's VENUS observatory. We acknowledge the use of code developed by M. Reidenbach for turbulence dissipation derivations. Other contributors to the

instrumentation development, execution of the experiment, and data recovery were R. Lueck, K. Bartlett and P. Macoun.

Appendix A. Supplementary data

Supplementary data to this article can be found online at https://doi.org/10.1016/j.ecss.2020.106815.

References

Anderson, J.J., Devol, A.H., 1973. Deep water renewal in Saanich Inlet, an intermittently anoxic basin. Estuar. Coast Mar. Sci. 1, 1–10.

Attard, K.M., Glud, G.N., McGinnis, D.F., Rysgaard, S., 2014. Seasonal rates of benthic primary production in a Greenland fjord measured by aquatic eddy correlation. Limnol. Oceanogr. 59, 1555–1569. https://doi.org/10.4319/lo.2014.59.5.1555.

Attard, K.M., Rodil, I.F., Berg, P., Norkko, J., Norkko, A., Glud, R.N., 2019. Seasonal metabolism and carbon export potential of a key coastal habitat: the perennial canopy-forming macroalga *Fucus vesiculous*. Limnol. Oceanogr. 64, 149–163. https://doi.org/10.1002/lno.11026.

Belley, R., Snelgrove, P.V.R., Archambault, P., Juniper, S.K., 2016. Environmental drivers of benthic fluxes variation and ecosystem functioning in Salish Sea and Northeast Pacific sediments. PLoS One. https://doi.org/10.1371/journal.pone.0151110.

Berg, P., Glud, R.N., Hume, A., Stahl, H., Oguri, K., Meyer, V., Kitazato, H., 2009. Eddy correlation measurements of oxygen uptake in deep ocean sediments. Limnol Oceanogr. Methods 7, 576–584.

Berg, P., Koopmans, D.J., Huettel, M., Li, H., Mori, K., Wüest, A., 2016. A new robust oxygen-temperature sensor for aquatic eddy covariance measurements. Limnol Oceanogr. Methods 14 (3), 151–167. https://doi.org/10.1002/lom3.10071.

Berg, P., Røy, H., Janssen, F., Meyer, V., Jørgensen, B.B., Huettel, M., de Beer, D., 2003. Oxygen uptake by aquatic sediments measured with a novel non-invasive eddy correlation technique. Mar. Ecol. Prog. Ser. 261, 75–83. https://doi.org/10.3354/meps261075.

Berg, P., Røy, H., Wiberg, P.L., 2007. Eddy correlation flux measurements: the sediment surface area that contributes to the flux. Limnol. Oceanogr. 52, 1672–1684.

Berg, P., Long, M.H., Huettel, M., Rheuban, J.E., McGlathery, K., others, 2013. Eddy correlation measurements of oxygen fluxes in permeable sediments exposed to varying current flow and light. Limnol. Oceanogr. 58, 1329–1343. https://doi.org/10.4319/lo.2013.58.4.1329.

Bertrand, S., Hughen, K., Sepulveda, J., Pantoja, S., Lange, C., 2012. Geochemical composition of surface sediments from the fjords of Northern Chilean Patagonia (44-47°S): spatial variability and implications for paleoclimate reconstructions. Geochem. Cosmochim. Acta 76, 125–146.

Bluteau, C.E., Ivey, G.N., Donis, D., McGinnis, D.F., 2018. Determining near-bottom fluxes of passive tracers in aquatic environments. Geophys. Res. Lett. 45, 2716–2725.

Brand, A., McGinnis, D.F., Wehrli, B., Wuest, A., 2008. Intermittent oxygen flux from the interior into the bottom boundary of lakes as observed by eddy correlation. Limnol. Oceanogr. 53, 1997–2006. https://doi.org/10.4319/lo.2008.53.5.1997.

Bryant, L.D., Lorrai, C., F McGinnis, D., Brand, A., Wüest, A., Little, J.C., 2010. Variable sediment oxygen uptake in response to dynamic forcing. Limnol. Oceanogr. 55, 950–964.

Cai, W.-J., Sayles, F.L., 1996. Oxygen penetration depths and fluxes in marine sediments. Mar. Chem. 52, 123–131.

Canfield, D.E., 1989. Sulfate reduction and oxic respiration in marine sediments: implications for organic carbon preservation in euxinic environments. Deep-Sea Res. 36, 121–138.

Chu, J.W.F., Tunnicliffe, V., 2015. Oxygen limitations on marine animal distributions and the collapse of epibenthic community structure during shoaling hypoxia. Global Change Biol. 21, 2989–3004.

Crusius, J., Berg, P., Koopmans, D.J., Erban, L., 2008. Eddy correlation measurements of submarine groundwater discharge. Mar. Chem. 109, 77–85. https://doi.org/10.1016/j.marchem.2007.12.004.

Davis, K.A., Monismith, S.G., 2011. The modification of bottom boundary layer turbulence and mixing by internal waves shoaling on a barrier reef. J. Phys. Oceanogr. 41, 2223–2241.

Dewey, R., Round, A., Macoun, P., Vervynck, J., Tunnicliffe, V., 2007. The VENUS cabled observatory: engineering meets science on the seafloor. OCEANS 2007 Conference Paper. https://doi.org/10.1109/OCEANS.2007.4449171, 0-933957-35-1.

Else, B.G.T., Rysgaard, S., Attard, K., Campbell, K., Crabeck, O., Galley, R.J., Geilfus, N.-X., Lemes, M., Lueck, R., Papakyriakou, T., Wang, F., 2015. Under-ice eddy covariance flux measurements of heat, salt, momentum, and dissolved oxygen in an artificial sea ice pool. Cold Reg. Sci. Technol. 119, 158–169.

Fang, X., Stefan, H.G., 1996. Dynamics of heat exchange between sediment and water in a lake. Water Resour. Res. 32, 1719–1727.

Favali, P., Beranzoli, L., 2006. Seafloor observatory science: a review. Ann. Geophys. 49, 515–567.

Gargett, A.E., Stucchi, D., Whitney, F., 2003. Physical processes associated with high primary production in Saanich Inlet, British Columbia. Estuar. Coast Shelf Sci. 56, 1141–1156.

Gasbarro, R., Chu, J.W.F., Tunnicliffe, V., 2019. Disassembly of an epibenthic assemblage in a sustained severely hypoxic event in a northeast Pacific basin. J. Mar. Syst. 198, 103184.

Glud, R.N., 2008. Oxygen dynamics of marine sediments. Mar. Biol. Res. 4, 243–289.

Glud, R.N., Stahl, H., Berg, P., Wenzhöfer, F., Oguri, K., Kitazato, H., 2009. In situ microscale variation in distribution and consumption of O_2: a case study from a deep ocean margin sediment (Sagami Bay, Japan). Limnol. Oceanogr. 54, 1–12.

Glud, R.N., Berg, P., Stahl, H., Hume, A., Larsen, M., Eyre, B.D., Cook, P.L.M., 2016. Benthic carbon mineralization and nutrient turn-over in a Scottish loch: an integrative in situ study. Aquat. Geochem. 22, 443–467.

Goring, D.G., Nikora, V.I., 2002. Despiking acoustic Doppler velocimeter data. J. Hydraul. Eng. 128, 117–126.

Goto, S., Matsubayashi, O., 2009. Relations between thermal properties and the porosity of sediments in the eastern flank of Juan de Fuca Ridge. Earth Planets Space 61, 863–870.

Grundle, D.S., Timothy, D.A., Varela, D.E., 2009. Variations of phytoplankton productivity and biomass over an annual cycle in Saanich Inlet, a British Columbia fjord. Continent. Shelf Res. 29, 2257–2269.

Hamme, R.C., Berry, J.E., Klymak, J.M., Denman, K.L., 2015. In situ O_2 and N_2 measurements detect deep-water renewal dynamics in seasonally-anoxic Saanich Inlet. Continent. Shelf Res. 106, 107–117. https://doi.org/10.1016/j.csr.2015.06.012.

Holtappels, M., Glud, R.N., Donis, D., Liu, B., Hume, A., Wenzhöfer, F., Kuypers, M.M., 2013. Effects of transient bottom water currents and oxygen concentrations on benthic exchange rates as assessed by eddy correlation measurements. J. Geophys. Res. Oceans 118, 1157–1169. https://doi.org/10.1002/jgrc.20112.

Holtappels, M., Kuyers, M.M.M., Schlüter, M., Volker Brüchert, V., 2011. Measurement and interpretation of solute concentration gradients in the benthic boundary layer. Limnol Oceanogr. Methods 9, 1–13. https://doi.org/10.4319/lom.2011.9.1.

Holtappels, M., Noss, C., Hancke, K., Cathalot, C., McGinnis, D.F., Lorke, A., Glud, R.N., 2015. Aquatic eddy correlation: quantifying the artificial flux caused by stirring-sensitive O_2 sensors. PLoS One 10 (1), e0116564.

Hyndman, R.D., Wang, K., 1993. Thermal constraints on the zone of major thrust earthquake failure: the Cascadia Subduction Zone. J. Geophys. Res. Solid Earth 98, 2039–2060.

Iriarte, J.L., 2018. Natural and human influences on marine processes in Patagonian subarctarctic coastal waters. Front. Mar. Sci. 5 https://doi.org/10.3389/fmars.2018.00360 article 360.

Jackson, J., Johnson, G.C., Dosser, H.V., Ross, T., 2018. Warming from recent marine heatwave lingers in deep British Columbia fjord. Geophys. Res. Lett. 45 https://doi.org/10.1029/2018GL078971.

Jørgensen, B.B., Boudreau, B., 2001. Diagenesis and sediment water exchange. In: Boudreau, B., Jørgensen, B.B. (Eds.), The Benthic Boundary Layer. Oxford University Press, New York, pp. 211–238.

Juniper, S.K., Brinkhurst, R.O., 1986. Water-column dark CO_2 fixation and bacterial-mat growth in intermittently anoxic Saanich Inlet, British Columbia. Mar. Ecol. Prog. Ser. 33, 41–50.

Katz, T., Yahel, G., Yahel, R., Tunnicliffe, V., Herut, B., Snelgrove, P., Crusius, J., Lazar, B., 2009. Groundfish overfishing, diatom decline, and the marine silica cycle: lessons from Saanich Inlet, Canada, and the Baltic Sea cod crash. Global Biogeochem. Cycles 23. https://doi.org/10.1029/2008GB003416.

Kunze, E., Dower, J.F., Beveridge, I., Dewey, R., Barlett, K.P., 2006. Observations of biologically generated turbulence in a coastal inlet. Science 313, 1768–1770.

Langton, S.J., Linsley, B.K., Robinson, R.S., Rosenthal, Y., Oppo, D.W., Eglinton, T.I., Howe, S.S., Djajadihardja, Y.S., Syamsudin, F., 2008. 3500 yr record of centennial-scale climate variability from the Western Pacific Warm Pool. Geology 36, 795–798.

Levin, L.A., Ekau, W., Gooday, A.J., Jorissen, F., Middelburg, J.J., Naqvi, W., Neira, C., Rabalais, N.N., Zhang, J., 2009. Effects of natural and human-induced hypoxia on coastal benthos. Biogeosciences 6, 2063–2098.

Long, M.H., Charette, M.A., Martin, W.R., McCorkle, D.C., 2015. Oxygen metabolism and pH in coastal ecosystems: eddy covariance hydrogen ion and oxygen exchange system (ECHOES). Limnol Oceanogr. Methods 13, 438–450.

Lorke, A., McGinnis, D.F., Maeck, A., 2013. Eddy-correlation measurements of benthic fluxes under complex flow conditions: effects of coordinate transformations and averaging time scales. Limnol Oceanogr. Methods 11, 425–437.

Lorrai, C., McGinnis, D.F., Berg, P., Brand, A., Wuest, A., 2010. Application of oxygen eddy correlation in aquatic systems. J. Atmos. Ocean. Technol. 27, 1533–1546.

Matabos, M., Tunnicliffe, V., Juniper, S.K., Dean, C., 2012. A year in hypoxia: epibenthic community responses to severe oxygen deficit at a subsea observatory in a coastal inlet. PLoS One 7, e45626.

Matabos, M., Piechaud, N., de Montigny, F., Sarradin, P.-M., Jozee, S., 2015. The VENUS cabled observatory as a method to observe fish behaviour and species assemblages in a hypoxic fjord, Saanich Inlet (British Columbia, Canada). Can. J. Fish. Aquat. Sci. 72, 24–26.

Matsumoto, E., Wong, C.S., 1977. Heavy metal sedimentation in Saanich Inlet measured with the 210Pb technique. J. Geophys. Res. 82, 5477–5482.

McCann-Grosvenor, K., Reimers, C.E., Sanders, R.D., 2014. Dynamics of the benthic boundary layer and seafloor contributions to oxygen depletion on the Oregon inner shelf. Continent. Shelf Res. 84, 93–106.

McGinnis, D.F., Sommer, S., Lorke, A., Glud, R.N., Linke, P., 2014. Quantifying tidally driven benthic oxygen exchange across permeable sediments: an aquatic eddy correlation study. J. Geophys. Res. Oceans 119, 6918–6932. https://doi.org/10.1002/2014JC010303.

Reeburgh, W.S., 1983. Rates of biogeochemical processes in anoxic sediments. Annu. Rev. Earth Planet Sci. 11, 269–298.

Reidenbach, M.A., Monismith, S.A., Koseff, J.R., Yahel, G., Genin, A., 2006. Boundary layer turbulence and flow structure over a fringing coral reef. Limnol. Oceanogr. 51, 1956–1968.

Reimers, C.E., Özkan-Haller, H.T., Berg, P., Devol, A., McCann-Grosvenor, K., Sanders, R. D., 2012. Benthic oxygen consumption rates during hypoxic conditions on the

Oregon continental shelf. J. Geophys. Res. Oceans 117, C02021. https://doi.org/10.1029/2011JC007564.

Reimers, C.E., Özkan-Haller, H.T., Sanders, R.D., McCann-Grosvenor, K., Chace, P.J., Crowe, S.A., 2016. The dynamics of benthic respiration at a mid-shelf station off Oregon. Aquat. Geochem. 22, 505–527. https://doi.org/10.1007/s10498-016-9303-5.

Rheuban, J.E., Berg, P., McGlathery, K.J., 2014. Multiple timescale processes drive ecosystem metabolism in eelgrass (*Zostera marina*) meadows. Mar. Ecol. Prog. Ser. 507, 1–13.

Rousseau, S., Kunze, E., Dewey, R., Bartlett, K., Dower, J., 2010. On turbulence production by swimming marine organisms in the open ocean and coastal waters. J. Phys. Oceanogr. 40, 2017–2121. https://doi.org/10.1175/2010JPO4415.1.

Sato, M., Klymak, J.M., Kunze, E., Dewey, R., Dower, J.F., 2014. Turbulence and internal waves in Patricia bay, Saanich inlet, British Columbia. Continent. Shelf Res. 85, 153–167.

Shaw, W.J., Trowbridge, J.H., 2001. The direct estimation of near-bottom turbulent fluxes in the presence of energetic wave motions. J. Atmos. Ocean. Technol. 18, 1540–1557.

Shaw, W.J., Trowbridge, J.H., Williams III, A.J., 2001. Budgets of turbulent kinetic energy and scalar variance in the continental shelf bottom boundary layer. J. Geophys. Res. 106, 9551–9564.

Smith, N.P., 2002. Observations and simulations of water-sediment heat exchange in a shallow coastal lagoon. Estuaries 25, 483–487.

Smith, R.W., Bianchi, T.S., Allison, M., Savage, C., Galy, V., 2015. High rates of organic carbon burial in fjord sediments globally. Nat. Geosci. 8, 450–453.

Stranne, C., O'Regan, M., 2015. Conductive heat flow and nonlinear geothermal gradients in marine sediments-observations from Ocean Drilling Program boreholes. Geo Mar. Lett. https://doi.org/10.1007/s00367-015-0425-3.

Syvitski, J.P.M., Burrell, D.C., Skei, J.M., 1987. Fjords: Processes and Products. Springer-Verlag, New York, p. 215.

Timothy, D. A. and M. Y. S. Soon. Primary production and deep-water oxygen content of two British Columbian fjords. Mar. Chem. 73: 37-51.

Tunnicliffe, V., 2000. A fine-scale record of 130 years of organic carbon deposition in an anoxic fjord, Saanich Inlet, British Columbia. Limnol. Oceanogr. 45 (6), 1380–1387. https://doi.org/10.4319/lo.2000.45.6.1380.

Walter, R.K., Squibb, M.E., Woodson, C.B., Koseff, J.R., Monismith, S.G., 2014. Stratified turbulence in the nearshore coastal ocean: dynamics and evolution in the presence of internal bores. J. Geophys. Res. 119, 8709–8730.

Yahel, G., Yahel, R., Katz, T., Lazar, B., Herut, B., Tunnicliffe, V., 2008. Fish activity: a major mechanism for sediment resuspension and organic matter remineralization in coastal marine sediments. Mar. Ecol. Prog. Ser. 372, 195–209.